Journal of Catalysis **187,** 506–517 (1999)
Article ID jcat.1999.2640, available online at http://www.idealibrary.com on IDEAL®

The Active Phase of Iron Catalysts for Acetonitrile Synthesis

Manish V. Badani and W. Nicholas Delgass[1]

School of Chemical Engineering, Purdue University, West Lafayette, Indiana 47907–1283

Received July 2, 1999; accepted July 15, 1999

In situ **Mössbauer spectroscopy has been used to examine the active phase of two different reduced 4% Fe/SiO_2 catalysts for acetonitrile synthesis from CO, H_2, and NH_3. The Fe^0-containing, silica-supported catalyst starts with a finite initial activity and displays a maximum in activity with time that tracks the amount of the ε'-$Fe_{2.2}C$ phase, indicating it as the active phase of the catalyst. The silica-supported catalyst containing Fe^{2+} only starts with a low activity and slowly rises to a stable activity but shows little change in the bulk structure of the catalyst. In this case, much of the change occurs on the surface of the catalyst and could not be monitored with Mössbauer spectroscopy. An increase in the reducibility of iron with time was confirmed, however, with H_2 desorption experiments. For reduced 11.9% Fe/carbon, also known to have ε'-$Fe_{2.2}C$ as the active phase for acetonitrile synthesis, spectra collected at cryogenic temperatures after 3 and 10 min of reaction indicate the following order in carbide formation: $Fe^0 \rightarrow \varepsilon' \rightarrow \chi \rightarrow \theta$. Transient mass spectrometry used to monitor the product stream in the first 5 min of reaction indicates that carbide formation precedes product formation. Reactions carried out over rereduced, postreaction 11.9% Fe/carbon indicate large-scale sintering during the first cycle of reaction. Mössbauer studies also show a rapid rearrangement of the bulk structure of the rereduced used catalyst when it is reintroduced to the reaction environment.**

INTRODUCTION

The synthesis of acetonitrile from CO, H_2, and NH_3 at high temperatures over transition metal catalysts is patented by Monsanto (1–3). According to Olivé and Olivé, Mo and Fe are the preferred catalysts. Work done earlier in our laboratory at 698–723 K over supported iron catalysts indicated that the Fe^0 and Fe_2N silica-supported catalysts displayed a significant initial activity which then reached a maximum and decayed at longer reaction times (4). The Fe^{2+}-only silica-supported catalyst, however, had almost no activity at the beginning of the reaction but slowly activated in the reaction mixture to a stable activity (4). The reduced 11.9% Fe-on-carbon (CSX203) catalyst, which was composed of mainly small particle (s.p.) Fe^0, started with an initial high activity that dropped sharply in first couple of hours of reaction and was followed by slight decay in activity at higher reaction times.

The different activity patterns observed on different catalysts were attributed to the changes in the active phase during the course of reaction. The Fe^0- and Fe_2N-containing catalysts, which show significant initial activity, are known to form carbides readily. The irreducible Fe^{2+}-containing catalyst, which cannot form a carbide directly, starts with an initial low activity. It is also known that small iron particles favor the formation of ε' carbide while the larger particles prefer to form χ carbide (5–9). Furthermore, at high temperatures (around 673 K), the ε' carbide is unstable and is converted to χ and θ carbides (8, 10–12). All the above facts indicate that there may be some correlation between the different activity patterns observed on different catalysts and their tendencies to form various carbides under reaction conditions.

In situ Mössbauer spectroscopy, used earlier to monitor changes in the bulk phase of the carbon-supported catalyst during the course of reaction, established ε'-$Fe_{2.2}C$ as the active phase of that catalyst (13). In the work reported here, similar studies were conducted on silica-supported catalysts where the activity patterns differ significantly depending on the initial state of the catalysts. In the previous work over the carbon-supported catalyst, the role of metallic iron for the product formation at the beginning of the reaction was not clear. Transient mass spectrometry used here to monitor the product formation during the first several minutes of reaction indicates that carbide formation precedes nitrile and hydrocarbon product formation.

In addition, this paper presents Mössbauer studies of the order of carbide phase formation and the regeneration of the carbon-supported catalyst.

EXPERIMENTAL METHODS

Catalyst preparation. Two silica-supported catalysts, designated 4% Fe/SiO_2 (calcined) and 4% Fe/SiO_2 (reduced), were prepared in separate batches by incipient wetness impregnation of dried Cab-O-Sil EH-5 silica with aqueous ferric nitrate [$Fe(NO_3)_3 \cdot 9H_2O$, Fischer] solution. The Fe/SiO_2 (reduced) reported here is the same as the Fe/SiO_2 (A) reported earlier (4). The impregnated catalysts

[1] To whom correspondence should be addressed. Fax: (765) 494–0805. E-mail: delgass@ecn.purdue.edu.

0021-9517/99 $30.00

were dried under ambient conditions for at least 2 weeks. The catalysts were further dried in a vacuum oven with the temperature raised stepwise to 475 K over an 8-h period and held at 475 K for 16 h. After vacuum drying, the catalysts were loaded into a tube furnace. The Fe/SiO_2 (calcined) catalyst was prepared by decomposing the ferric nitrate salt in O_2 at 573 K for 3 h. For the Fe/SiO_2 (reduced) catalyst, the decomposition was carried out in an H_2 atmosphere. In the latter case, after cooling down to room temperature, the catalyst was passivated with 1% O_2/He before exposure to air.

The 11.9% Fe/carbon catalyst was prepared by using a high-purity, high-surface-area amorphous carbon black, CSX203, supplied by Cabot Corporation. Prior to impregnation, the support was desulfurized by heating it for 12 h at 1223 K in flowing H_2 (14). This reduced the sulfur content of the CSX203 from 6550 to 1860 ppm, as determined by X-ray fluorescence. The desulfurized support was impregnated with aqueous ferric nitrate solution, forming the 11.9 wt% Fe/carbon catalyst. In this case the iron nitrate was decomposed in H_2 in a manner similar to that described above for the Fe/SiO_2 (reduced) catalyst. The carbon-supported catalyst reported here is the same as that reported in earlier work (13).

Before reaction, the catalysts were reduced in H_2 at 673 K. The reduction time was 12 h for silica-supported catalysts and 16 h for carbon-supported catalysts. After reduction, the catalyst was taken to reaction temperature, 698 K, in H_2 and the reaction was initiated by switching from H_2 to the reaction mixture.

Kinetics. The long-term steady-state experiments were carried out in a differential U-tube reactor. The catalyst-filled reactor was attached to the gas manifold with Cajon Ultra-Torr O-ring fittings and heated in a fluidized sand bath. The catalyst temperature was measured by a thermocouple located just outside the wall of the reactor. The product stream was analyzed using a Waters Dimension-I gas chromatograph interfaced with an IBM PC. The $\frac{1}{8}$-in.-diameter Hayesep Q column was 10 ft long and the chromatograph was equipped with a Valco pneumatically operated sampling valve and a temperature-controlled sample loop.

The transient experiments were carried out in a straight quartz tube placed within a brass sheathing along with two chromel–alumel thermocouples next to the reactor wall for temperature control. The reactor was heated by a Research Incorporated IR oven and controlled by a Micristar temperature controller. Gases could flow from any of three manifolds to the reactor or through a bypass that facilitated calibration of the reactor stream. The effluent of the reactor or bypass was analyzed by an Extrel Corporation EMBA II modulated beam quadrupole mass spectrometer interfaced to a Digital Equipment Corporation MINC-11 minicomputer for data acquisition.

Mössbauer spectroscopy. The Mössbauer experiments were conducted in an *in situ* high-temperature absorber cell constructed from corrosion-resistant Haynes 230 alloy following a design used previously (15). The Haynes 230 alloy is a nickel–chromium–tungsten–molybdenum alloy that combines excellent high-temperature strength, long-term thermal stability, and outstanding resistance to oxidizing and nitriding environments and is thus suitable for the acetonitrile synthesis reaction. The catalysts were pressed into self-supporting wafers and mounted in the cell, which was then bolted together. Once the cell stabilized at reaction temperature in H_2, the reaction was initiated by switching from H_2 to a mixture of $1:2:1$ $CO:H_2:NH_3$. The effluent of the cell was analyzed by the Waters gas chromatograph. After a fixed reaction time, the GC point was taken, the reaction mixture was immediately replaced by He, and the temperature of the cell was lowered. The cell was cooled to room temperature and the spectrum was collected in the He atmosphere. For the next segment of reaction, the cell was heated to reaction temperature in He and the above procedure repeated for the next spectrum. This procedure allowed sequential monitoring of the activity of the catalyst and the changes in the bulk characteristics of the catalyst as a function of reaction time. At times, the cell was cooled with liquid nitrogen and the spectrum collected at cryogenic temperature. This involved removing the cartridge heaters and installing a level indicator that maintained a constant level of liquid nitrogen in the central cylinder of the cell. As the cell was cooled, the pressure was adjusted to 1 atm by addition of He. Once the temperature stabilized at around 100 K, the data acquisition was initiated.

The constant-acceleration Mössbauer spectra were collected with an Austin Science S-600 spectrometer controller, a $^{57}Co/Rh$ source (25–100 mCi), and a PCA-II multichannel analyzer installed in the Zenith Z-159 computer. The binary data files written with the PCA-II data acquisition program were transferred to the mainframe computers where they were translated into more usable ASCII files. The files were then folded and fitted using a Levenberg–Marquardt least-squares routine, developed in our laboratory by Howsmon (16). The routine fits isomer shift, quadrupole splitting, hyperfine splitting, linewidth, total absorbance, and background, and in addition it allows for the evaluation of probability density for a hyperfine field distribution (17, 18). It also allows for optional constraints on isomer shift, quadrupole splitting, hyperfine field, and linewidth. For a six-line spectrum, to begin with, the intensity ratio of the pairs of peaks was maintained at $3:2:1$ with equal widths for all peaks. If necessary, the intensity ratio was maintained at $3:2:1$ allowing different linewidths for each pair. Only in rare cases were hyperfine parameters constrained to help deconvolute closely related or overlapping components of the spectrum. All the spectra reported

here have isomer shifts (ISs) referenced to a 25-μm NBS Fe foil spectrum.

The helium and hydrogen gases used were Matheson ultrahigh-purity grade and were passed through Scott oxygen purifiers before use. CO (Matheson UHP) was filled directly from the production facility into aluminum cylinders to minimize iron carbonyl contamination of the reactant gas. NH_3 was Matheson research purity grade and used without further purification.

RESULTS AND DISCUSSION

In earlier work (13), ε' iron carbide was found to be the active phase of the catalyst during acetonitrile synthesis over prereduced 11.9% Fe/carbon. In the present work the following aspects are discussed in more detail: the stability of ε' carbide, the order of carbide phase formation, the activity of the Fe^0 phase, the regeneration of spent catalyst, and the investigation of the active phase of reduced silica-supported catalysts. For the last case, catalysts with different particle size distributions were studied.

Active Phase of Reduced 11.9% Fe/Carbon

The Mössbauer spectra of reduced 11.9% Fe/carbon before reaction and after 10, 160, and 1510 min of reaction are shown in Fig. 1. The solid lines show the overall fit of the spectra. The parameters of the fit are given in Table 1. The prereduced catalyst consists mainly of small particle

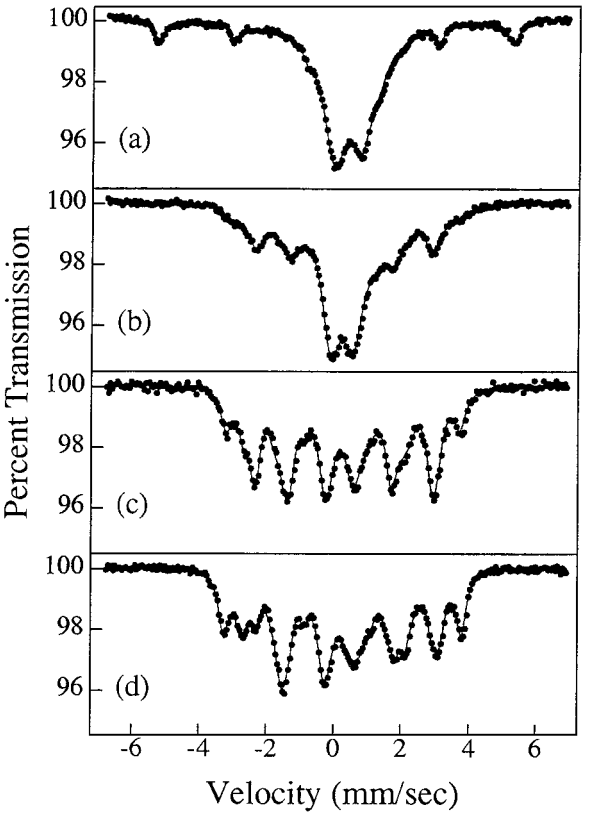

FIG. 1. Room-temperature Mössbauer spectra of prereduced 11.9% Fe/carbon after various reaction times: (a) $t = 0$ min, (b) $t = 10$ min, (c) $t = 160$ min, (d) $t = 1510$ min.

TABLE 1

Mössbauer Spectral Parameters Corresponding to Fig. 1 for Prereduced 11.9% Fe/Carbon after Various Reaction Times at 698 K

Fig.	Phase	IS (mm/s)	QS (mm/s)	HFS (kOe)	LW (mm/s)	Relative area (%)
1a	Fe^{2+}	1.0	—	—	1.0	28.6
	Fe^{3+}	0.31	0.82	—	0.38	12.2
	Fe^0	0.0	−0.01	327.7	0.41	15.4
	Fe^0	0.0	−0.07	0.0–248.4	0.26	43.8
1b	s.p. carbide	0.23	0.65	—	0.66	39.4
	Fe^{2+}	0.74	1.09	—	0.84	14.4
	ε'	0.25	0.02	162.0	0.55	27.3
	$\chi^{(I)}$	0.3	−0.09	181.2	0.44	5.4
	$\chi^{(II)}$	0.27	0.02	212.7	0.43	6.2
	$\chi^{(III)}$	0.12	0.01	102.7	0.50	7.3
1c	s.p. carbide	0.17	0.78	—	0.54	13.0
	ε'	0.22	0.06	163.8	0.39	35.6
	$\chi^{(I)}$	0.29	−0.09	179.0	0.40	16.3
	$\chi^{(II)}$	0.26	0.0	215.3	0.41	17.0
	$\chi^{(III)}$	0.12	0.02	102.6	0.48	18.1
1d	s.p. carbide	0.17	0.76	—	0.53	15.3
	ε'	0.18	0.12	163.8	0.36 : 0.27 : 0.47	16.3
	$\chi^{(I)}$	0.29	−0.09	182.6	0.43 : 0.33 : 0.69	26.3
	$\chi^{(II)}$	0.26	0.01	219.0	0.34 : 0.49 : 0.28	22.6
	$\chi^{(III)}$	0.12	0.0	105.5	0.32 : 0.41 : 0.46	19.5

Fe^0 which is fitted with a hyperfine field distribution with an average hyperfine field of 62 kOe. For small particle Fe^0, the anisotropy energy decreases and becomes comparable to thermal energy at room temperature. This leads to superparamagnetic relaxation and decreased magnetic splitting due to collective magnetic excitations (19). Around 15% of the iron spectral area has the form of a magnetically split six-line spectrum with a hyperfine field of 327.7 kOe, close to the bulk value of 330 kOe. In addition, there is another singlet with an IS of ca. 1.0 mm/s, corresponding to Fe^{2+}. This unusual Fe^{2+} singlet, characteristic of cancellation of the atomic and extraatomic field gradients, is documented for carbon-supported catalysts (20).

The postreaction spectra are fitted with ε' carbide, χ carbide, and superparamagnetic carbide species. Figure 2 displays the spectral areas of the ε' and superparamagnetic carbides and acetonitrile activity as a function of reaction time. The decay in acetonitrile activity over long periods of reaction matches very well the loss of ε' carbide (13). The initial sharp drop in activity is accompanied by conversion of superparamagnetic carbide to magnetically split ε' carbide.

To identify the fraction of the superparamagnetic carbide that is ε' carbide, Mössbauer spectra were also collected at lower temperature. Figure 3 shows the spectra at 102 K

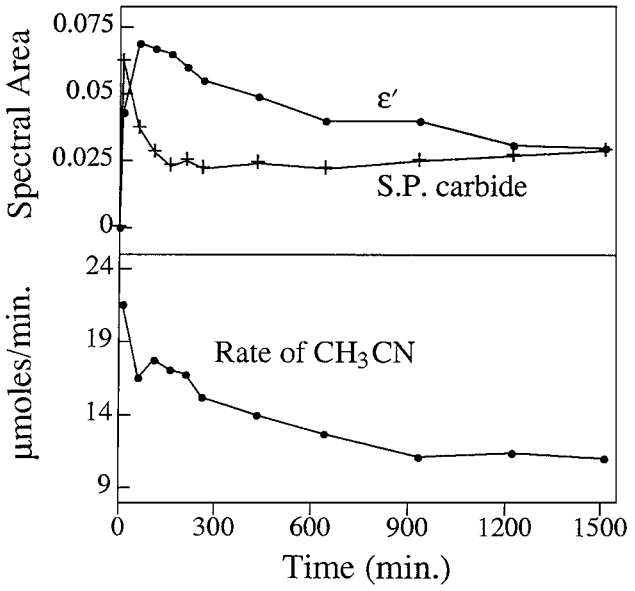

FIG. 2. Spectral areas and acetonitrile activity as a function of time on stream over prereduced 11.9% Fe/carbon.

after 10 and 1510 min of reaction. The parameters of the fits are listed in Table 2. As expected, the increased magnetic ordering at low temperature causes a loss in spectral area of the superparamagnetic phase and a corresponding gain in the peak areas of the magnetically split, ordered phases. Comparison of the areas of all phases at 298 K (Table 1) with those at 102 K (Table 2) indicates that after 10 min of reaction, the superparamagnetic carbide consists mainly of ε' with some χ carbide. After 1510 min of reaction, however, the superparamagnetic carbide includes some ε' as well as

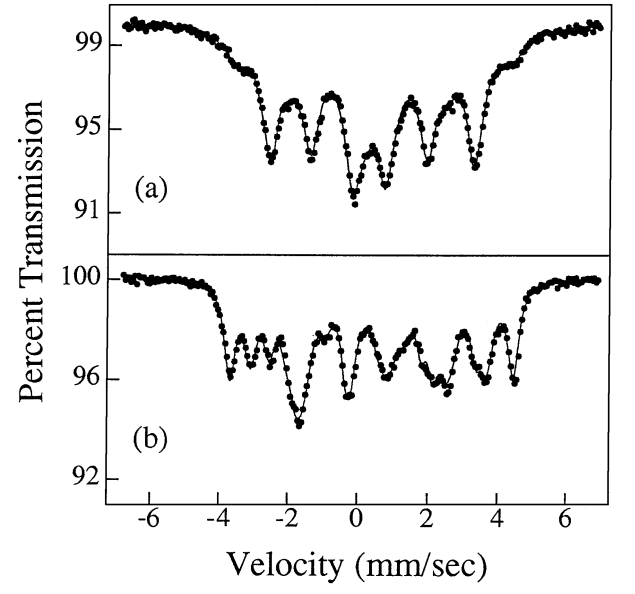

FIG. 3. Low-temperature (102 K) spectra of prereduced 11.9% Fe/carbon after (a) 10 min and (b) 1510 min of reaction at 698 K.

TABLE 2

Mössbauer Spectral Parameters Corresponding to Fig. 3 for Prereduced 11.9% Fe/Carbon after 10 and 1510 min of Reaction at 698 K

Fig.	Phase	IS (mm/s)	QS (mm/s)	HFS (kOe)	LW (mm/s)	Relative area (%)
3a	s.p. carbide	0.31	0.93	—	0.60	15.2
	Fe^{2+}	1.05	1.65	—	0.73	9.1
	ε'	0.35	0.04	180.4	0.46	32.1
	$\chi^{(I)}$	0.48	−0.11	196.3	0.45	7.2
	$\chi^{(II)}$	0.35	0.06	244.1	0.94	18.2
	$\chi^{(III)}$	0.22	0.43	141.8	1.48	18.2
3b	s.p. carbide	0.3	0.96	—	0.28	5.0
	ε'	0.27	0.15	183.7	0.39 : 0.32 : 0.27	17.8
	$\chi^{(I)}$	0.41	−0.11	210.5	0.46 : 0.43 : 0.75	27.1
	$\chi^{(II)}$	0.36	0.02	252.8	0.39 : 0.49 : 0.34	29.5
	$\chi^{(III)}$	0.20	−0.01	121.8	0.37 : 0.51 : 0.6	20.6

χ carbide, but there is an additional species in the high-field region (≈250 kOe at 100 K), which we assign on basis of hyperfine field to θ-Fe_3C carbide.

Based on the above results, for carbon-supported catalysts, the loss in activity is caused first by sintering of the ε' phase (as indicated by the superparamagnetic to magnetically split transformation in the first hour) and then by conversion to lower-carbon-content χ and θ carbides. This latter conversion leads to loss of carbon from the lattice, contributing to carbon overlayers on the surface of the catalyst. In the spectra discussed above, the amount of the $\chi^{(III)}$ component of the χ phase is higher than that expected from the theoretical ratio of $\chi^{(I)}:\chi^{(II)}:\chi^{(III)} = 2:2:1$. This change in ratio may be a result of relaxation phenomena (21) or the presence in the carbide of some nitrogen, which lowers the hyperfine field. The other possibility is the presence of an iron carbide with carbon content between those of ε' and χ carbide. Le Caër *et al.* reported the presence of Fe_xC_{1-x} carbide with continuously changing carbon content from $x = 0.29$ to $x = 0.32$ (22). They reported that the proportion of the $\chi^{(III)}$-related component increases with increase in carbon content. The uncertainty in assignment of the χ carbide component, however, does not change the conclusion that ε' carbide is the active phase of the catalyst since the highest activity is associated with materials having a single magnetically split component in the ε' region.

Stability of ε'-Iron Carbide

The conversion of ε' to χ and θ indicates instability of ε' carbide at high temperatures as has been reported earlier (8, 10–12). Further studies were conducted by heating the ε' carbide in He at 698 K, the reaction temperature. Figure 4 shows the spectra of reduced 11.9% Fe/carbon after 50 min of reaction followed by heating in He at 698 K for 15 h. The parameters of the fit are given in Table 3. As seen

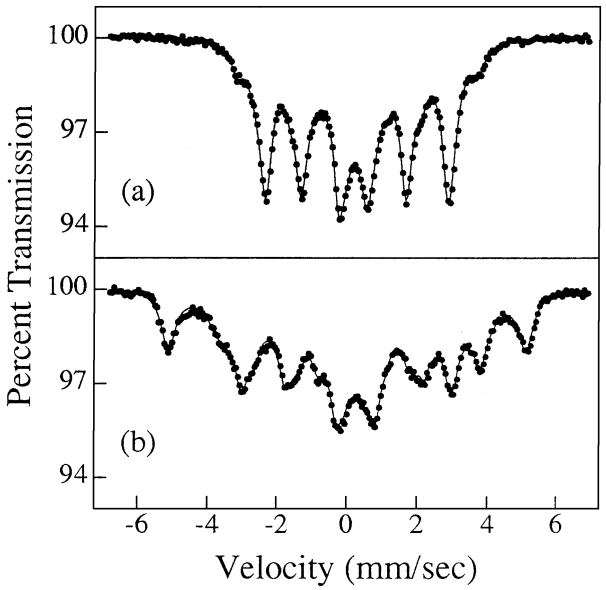

FIG. 4. Room-temperature Mössbauer spectra of prereduced 11.9% Fe/carbon (a) after 50 min of reaction at 698 K and (b) after heating (a) in He for 15 h at 698 K.

from the loss of intensity of the main six-line pattern in Fig. 4b compared with Fig. 4a and the gain in intensity at higher velocities, most of the ε' phase loses carbon to form lower-carbon-containing (higher hyperfine splitting) carbides. A significant amount of metallic iron is also formed by complete removal of carbon, as indicated by presence of species with the highest hyperfine field (318 kOe). This is consistent with thermodynamics which favors metallic iron over carbides at elevated temperature. The amount of "chemical stress" (strain energy) increases with the increase in amount of carbon in the carbide (23). Hence, the more unstable carbides will tend to lose carbon under reaction environment to form more stable carbides. These

TABLE 3

Mössbauer Spectral Parameters Corresponding to Fig. 4 for Prereduced 11.9% Fe/Carbon after 50 min of Reaction Followed by Heating in He for 15 h at 698 K

Fig.	Phase	IS (mm/s)	QS (mm/s)	HFS (kOe)	LW (mm/s)	Relative area (%)
4a	s.p. carbide	0.19	0.62	—	0.67	19.8
	ε'	0.24	0.04	161.6	0.42 : 0.35 : 0.31	40.4
	$\chi^{(I)}$	0.34	−0.13	172.5	0.68 : 0.47 : 0.50	18.2
	$\chi^{(II)}$	0.26	0.02	213.6	0.46 : 0.92 : 0.23	8.2
	$\chi^{(III)}$	0.12	−0.11	99.1	0.47 : 0.59 : 1.37	13.4
4b	s.p. carbide	0.18	0.61	—	0.83	15.6
	Fe^0	0.0	0.0	318.0	0.51	20.5
	$\chi^{(I)}$	0.25	−0.07	175.8	0.50 : 0.47 : 0.48	13.4
	$\chi^{(II)}$	0.30	0.08	212.7	0.33 : 0.26 : 0.46	6.5
	$\chi^{(III)}$	0.12	−0.03	103.3	0.52 : 0.47 : 0.52	12.2
	θ	0.19	−0.05	226.7	1.0 : 0.87 : 0.39	31.8

TABLE 4

Mössbauer Spectral Parameters Corresponding to Fig. 5 for Prereduced 11.9% Fe/Carbon after 3 min of Reaction at 698 K

Phase	IS (mm/s)	QS (mm/s)	HFS (kOe)	LW (mm/s)	Relative area (%)
s.p. carbide	0.3	0.81	—	0.68	22.7
Fe^{2+}	1.07	1.63	—	0.42	2.3
ε'	0.35	0.03	177.5	0.53	38.7
$\chi^{(I)}$	0.48	−0.15	197.7	0.61	9.6
$\chi^{(II)}$	0.35	−0.02	244.1	0.87	12.0
$\chi^{(III)}$	0.22	−0.14	99.1	1.0	14.7

qualitative conclusions are the main point of Fig. 4, but the fitting parameters given in Table 3 further support the finding that spectrum 4b represents decomposition of the carbide phases. The fit shown required an extra, broad six-line species with a hyperfine field of 226.7 kOe. Its high field relative to the $\chi^{(II)}$ species suggests the presence of θ carbide. Furthermore, the difficulty of fitting this spectrum is consistent with the disorder expected during carbon evolution from the bulk.

Order of Carbide Phase Formation

At longer reaction times and when heated in inert atmosphere, the ε' carbide converts to metallic iron following the path of decreasing carbon content; $\varepsilon' \rightarrow \chi \rightarrow \theta \rightarrow Fe^0$. The question thus arises whether the Fe^0 catalyst goes through different carbide phases of increasing carbon content or whether there is a direct conversion of Fe^0 to ε'. As shown in Table 2, after 10 min of reaction the catalyst has a significant amount of χ and θ carbides, in addition to ε' carbide. To investigate the order of carbide formation, spectra were collected at room temperature and liquid nitrogen temperature after 3 min of reaction. The room-temperature spectrum was composed mostly of superparamagnetic carbide, but the liquid nitrogen spectrum (Fig. 5) was well resolved into magnetically split phases. The parameters of the fit along with the relative areas of different phases are listed in Table 4. Comparison of parameters of Fig. 5 with

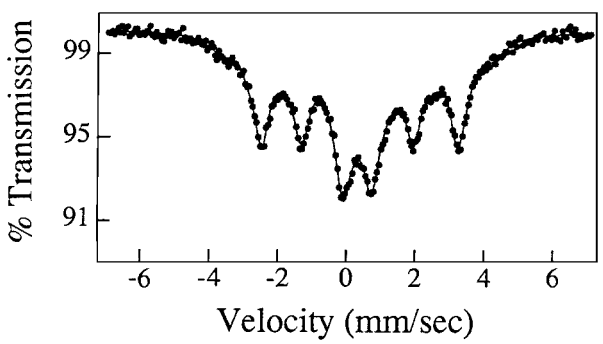

FIG. 5. Low-temperature (102 K) Mössbauer spectrum of prereduced 11.9% Fe/carbon after 3 min of reaction at 698 K.

those for Fig. 3a (low temperature, 10-min spectrum) clearly shows that the proportion of ε' is higher after 3 min of reaction than after 10 min of reaction. This is in contrast to results obtained by Tau *et al.* on 10% Fe/Al_2O_3 for Fischer–Tropsch synthesis at 543–558 K, where the χ form exceeds the ε' form during initial stages of the reaction (10). In our case, the metallic iron is first converted to ε' (a higher-carbon-containing carbide) which then reverts to χ and θ (lower-carbon-containing carbides). Similar observations were made during annealing of steel where Fe^0 is found to convert first to ε' carbide (24).

Activity of Fe^0

Although Fig. 3a shows little Fe^0 after 10 min of reaction, the high initial activity observed over that period leaves the question of Fe^0 activity unresolved. To investigate the activity of Fe^0, a transient step-change experiment was performed over prereduced 11.9% Fe/carbon. After prereduction, the flow stream was switched from H_2 to a mixture of 1:2:1:1 $CO:H_2:NH_3$:He at 723 K and the effluent of the reactor was analyzed with the mass spectrometer. Figure 6 shows the products that were observed during the first 5 min of the reaction. As seen, in first 20 s of the reaction (the start of reaction is indicated by the rise of the He signal), CO_2 was formed with a high initial rate, suggesting that the Bouduard reaction ($2CO \rightarrow C + CO_2$) dominates all other reactions on Fe^0. The free carbon formed during this reaction is used in the formation of iron carbides, after which formation of nitriles and other hydrocarbons starts.

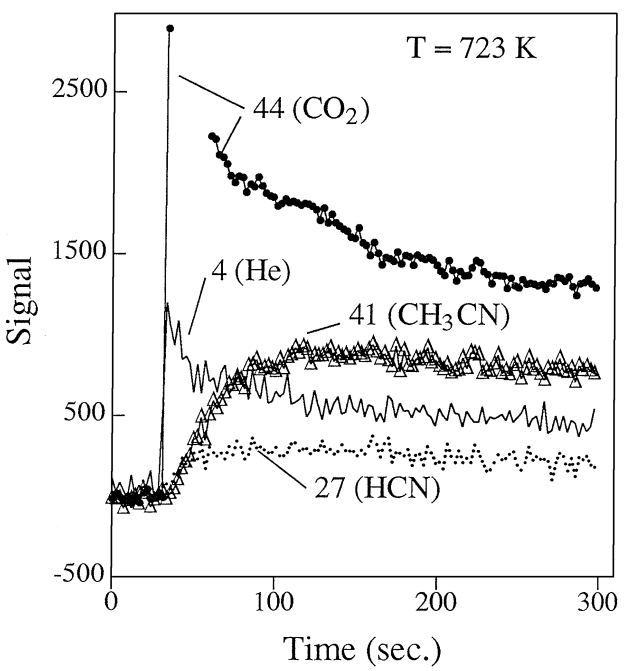

FIG. 6. Mass spectral analysis of a step change from H_2 to 1:2:1:1 $CO:H_2:NH_3$:He over reduced 11.9% Fe/carbon at 723 K.

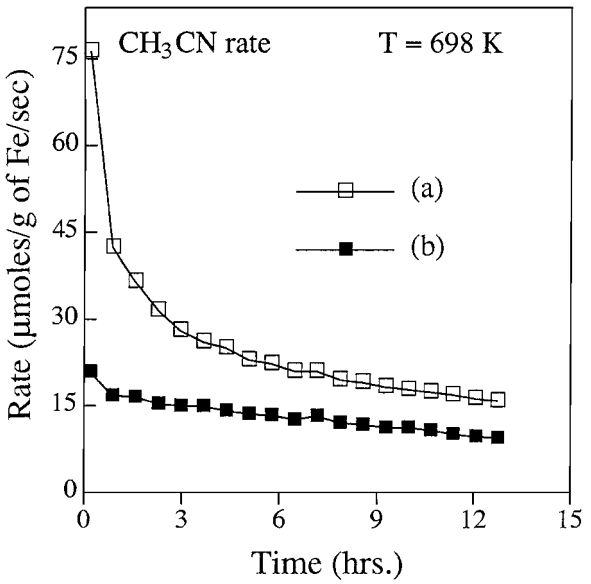

FIG. 7. Reaction of $CO:2H_2:NH_3$:He at 698 K: (a) reduced 11.9% Fe/carbon, (b) rereduced postreaction 11.9% Fe/carbon from (a).

Regeneration of 11.9% Fe/Carbon

Another aspect studied was the regeneration of used catalysts. Figure 7 shows long-term steady-state activity for freshly reduced 11.9% Fe/carbon and for a rereduced postreaction catalyst. After an initial reaction period of 24 h at 698 K on a reduced catalyst (although only the first 12 h of activity is shown), the catalyst was rereduced at 673 K for 16 h. As seen, rereducing the postreaction catalyst failed to enhance the specific rate significantly. The lower rate on the rereduced catalyst suggests sintering as the main cause of activity loss during the reaction. Sintering was confirmed using Mössbauer spectroscopy on a separate batch of catalyst. In this case, the catalyst was rereduced after 1510 min of reaction in the previous cycle in the Mössbauer cell (Fig. 1). Figure 8 shows the Mössbauer spectrum of rereduced 11.9% Fe/carbon along with spectra collected after 10, 100, and 230 min of further reaction. The parameters of the fits are given in Table 5. The rereduced catalyst has very little residual superparamagnetic carbide. Much of the rereduced catalyst is composed of metallic iron particles which are large in size as indicated by their hyperfine field of 330.7 kOe, close to the bulk value (330 kOe). In comparison, the original reduced catalyst had most of the iron in the form of small particle Fe^0. There were some larger particles, but their hyperfine field (327.7 kOe) was smaller than that observed for rereduced catalyst. Thus, Fig. 8a confirms significant sintering after the first cycle of reaction and rereduction.

Surprisingly, throughout the initial reaction period from the first 60 to 1510 min on the freshly reduced catalyst, the hyperfine fields of ε' and χ remained almost constant, indicating little sintering. But the hyperfine fields of ε' and χ on the rereduced catalyst are significantly higher

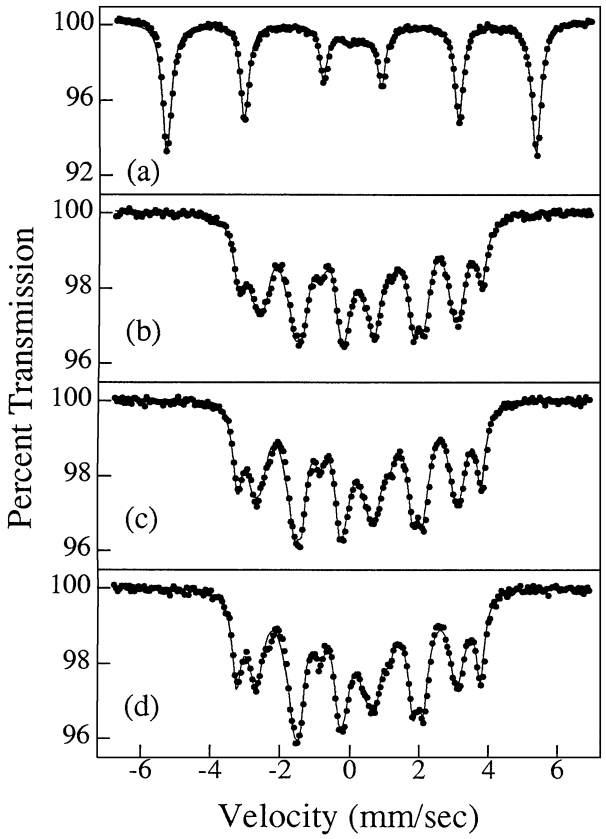

FIG. 8. Room-temperature Mössbauer spectra of rereduced postreaction 11.9% Fe/carbon after various reaction times: (a) $t = 0$ min, (b) $t = 10$ min, (c) $t = 100$ min, (d) $t = 230$ min.

compared with their counterparts on the reduced catalyst, consistent with larger particle size. This may indicate the removal of grain boundaries in the carbide particles during rereduction. In addition, the spectrum after 10 min of reaction over the rereduced catalyst has a closer resemblance to the spectrum expected after several hours of reaction over a freshly reduced catalyst. Tau *et al.* proposed that for Fischer–Tropsch reaction at 543 K, the restructuring caused by carburization, if undisturbed by high-temperature (ca. 730 K) reduction, maintains a solid that is more receptive to carburization (10). In our case, the rereduced postreaction catalyst also quickly carburizes on further reaction, returning to the form it had before the rereduction.

The fitting of the postreaction spectra for the rereduced catalyst was difficult because of their broad linewidths; however, the trend in reaction rate versus structure is clear. After 10 min of reaction on the rereduced catalyst, the acetonitrile rate went up to 15.9 μmol/min compared with 11 μmol/min after 1510 min of reaction on the reduced catalyst. Accompanying this slight increase in activity was an increase in amount of ε' carbide with simultaneous decrease in the amount of superparamagnetic carbide (probably mostly χ and θ based on the similarity of Figs. 1d and 8b) and magnetically split χ carbide as shown in Fig. 8b and Table 5. This agrees with the assertion that ε' is the active phase of the catalyst. After a further decrease in spectral area for ε' in Fig. 8c it goes up in value in Fig. 8d. This discrepancy is caused by the inclusion of some of the $\chi^{(I)}$ spectral area in ε'. This is indicated by the higher hyperfine field of ε' in Fig. 8d (178 kOe) compared with that in Figs. 8b and 8c (172 ± 2 kOe).

Silica-Supported Catalysts

In situ Mössbauer experiments were also carried out on silica-supported catalysts. The strong support interactions in these catalysts can cause much of the iron to remain in an oxide form even after reduction in H_2 at 673 K for 12 h. Figure 9 shows the specific rate of acetonitrile formation as a function of time on stream for reduced 4% Fe/SiO_2 (calcined) and 4% Fe/SiO_2 (reduced). The activity starts high on reduced 4% Fe/SiO_2 (calcined), reaches a maximum, and then decays. On reduced 4% Fe/SiO_2 (reduced), the initial activity is very low, but then it slowly rises during reaction and finally reaches a stable value. We have associated this behavior with iron reducibility (4). The activity maximum is characteristic of a catalyst containing large Fe^0 particles while the slow rise in activity represents a catalyst reducible only to Fe^{2+} in flowing H_2 at 673 K. The large Fe^0 particles in 4% Fe/SiO_2 (calcined) were formed by calcining the ferric nitrate-impregnated precursor in O_2 at 573 K for 3 h.

Active Phase of 4% Fe/SiO_2 (Calcined)

Figure 10 shows the room-temperature Mössbauer spectrum of reduced 4% Fe/SiO_2 (calc) along with the spectra

TABLE 5

Mössbauer Spectral Parameters Corresponding to Fig. 8 for Rereduced Postreaction 11.9% Fe/Carbon after Various Reaction Times at 698 K

Fig.	Phase	IS (mm/s)	QS (mm/s)	HFS (kOe)	LW (mm/s)	Relative area (%)
8a	s.p. carbide	0.21	0.73	—	0.60	10.6
	Fe^0	0.0	0.0	330.7	0.32 : 0.28 : 0.25	89.4
8b	s.p. carbide	0.17	0.58	—	0.81	11.2
	ε'	0.2	0.03	170.1	0.48 : 0.68 : 0.24	28.1
	$\chi^{(I)}$	0.27	−0.08	185.3	0.5 : 0.33 : 0.37	23.3
	$\chi^{(II)}$	0.22	0.06	216.9	0.33 : 0.44 : 0.21	18.2
	$\chi^{(III)}$	0.10	−0.01	105.6	0.34 : 0.49 : 0.33	19.2
8c	s.p. carbide	0.16	0.71	—	0.63	13.1
	ε'	0.19	0.03	172.2	0.42 : 0.65 : 0.26	19.6
	$\chi^{(I)}$	0.27	−0.07	185.9	0.46 : 0.29 : 0.54	25.3
	$\chi^{(II)}$	0.24	0.03	217.4	0.29 : 0.46 : 0.24	20.1
	$\chi^{(III)}$	0.10	−0.01	105.8	0.33 : 0.45 : 0.42	21.9
8d	s.p. carbide	0.18	0.71	—	0.65	13.7
	ε'	0.20	0.01	178.0	0.43 : 0.65 : 0.33	25.4
	$\chi^{(I)}$	0.28	−0.07	189.6	0.75 : 0.25 : 0.72	19.7
	$\chi^{(II)}$	0.24	0.03	217.6	0.27 : 0.51 : 0.23	18.8
	$\chi^{(III)}$	0.12	0.0	106.3	0.34 : 0.45 : 0.36	22.4

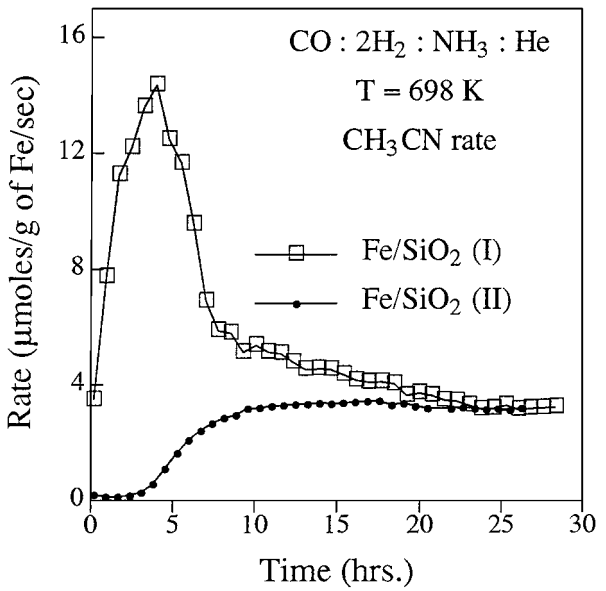

FIG. 9. Specific rate of acetonitrile synthesis as a function of time on stream over reduced 4% Fe/SiO_2 catalysts: (I) calcined, (II) reduced.

collected after 50, 160, and 750 min of reaction. The solid lines indicate the overall fit of the spectra and the parameters of the fit are given in Table 6. The spectral area of the reduced catalyst (Fig. 10a) is composed of around 20% metallic iron, with the balance made up of Fe^{2+} iron. The Fe^{2+} iron is composed of a high-coordination or bulk Fe^{2+} with a larger IS and quadrupole splitting (QS) and a low-coordination or surface Fe^{2+} with a smaller IS and QS (25). For the postreaction spectra, in addition to superparamagnetic carbide, ε' and χ carbide, high-coordination or bulk Fe^{2+} and of low-coordination or surface Fe^{2+} are present at lower reaction times. Figure 11 shows the spectral areas of the various phases and the acetonitrile activity as a function of time on stream. Compared with that for the carbon-supported catalysts, the fits for silica-supported catalysts are less accurate for several reasons. To begin with, much of the iron is present in an irreducible Fe^{2+} form which remains unchanged during reaction. Also, due to very small particle size, relaxation effects are more prominent, resulting in large quantities of superparamagnetic carbide and broadening of the overall spectra. The correspondingly smaller amounts of magnetically split ε' and χ carbides lead to larger errors in fitting those phases. Since both ε' and $\chi^{(I)}$ sites have similar hyperfine fields (~165–180 kOe at 298 K), the contribution of ε' is corrected by taking advantage of the fact that $\chi^{(I)}$ and $\chi^{(II)}$ should be present in the same amount. The corrected value of ε' is given by $\varepsilon'_c = \varepsilon' + \chi^{(I)} - \chi^{(II)}$ and it is this value that is plotted in Fig. 11. The relative spectral

TABLE 6

Mössbauer Spectral Parameters Corresponding to Fig. 10 for Prereduced 4% Fe/SiO_2 (Calcined) after Various Reaction Times at 698 K

Fig.	Phase	IS (mm/s)	QS (mm/s)	HFS (kOe)	LW (mm/s)	Relative area (%)
10a	Fe^{3+}	0.36	0.83	—	0.30	3.6
	Fe^{2+}	1.06	1.93	—	0.58	45.8
	Fe^{2+} (low coord)	0.94	1.27	—	0.64	29.8
	Fe^0	0.0	0.0	323.7	0.46	20.8
10b	Fe^{2+}	0.94	1.78	—	0.82	44.9
	s.p. carbide	0.24	0.64	—	0.67	13.5
	ε'	0.24	0.03	165.4	0.32	20.8
	$\chi^{(I)}$	0.39	−0.14	178.8	0.50	10.1
	$\chi^{(II)}$	0.25	0.07	206.9	0.67	6.5
	$\chi^{(III)}$	0.12	0.1	116.7	0.27	4.2
10c	Fe^{2+}	0.89	1.76	—	0.79	30.2
	s.p. carbide	0.18	0.77	—	0.66	13.3
	ε'	0.24	0.04	164.0	0.33	40.1
	$\chi^{(I)}$	0.35	−0.12	173.8	0.32	10.1
	$\chi^{(II)}$	0.25	0.05	217.6	0.32	3.0
	$\chi^{(III)}$	0.12	0.24	123.1	0.29	3.3
10d	Fe^{2+}	0.92	1.95	—	0.81	33.5
	s.p. carbide	0.22	0.48	—	0.92	30.5
	$\varepsilon' + \chi^{(I)}$	0.18	0.08	166.3	0.55	20.4
	$\chi^{(II)}$	0.25	0.05	220.2	0.62	8.3
	$\chi^{(III)}$	0.12	−0.29	70.0	0.40	7.3

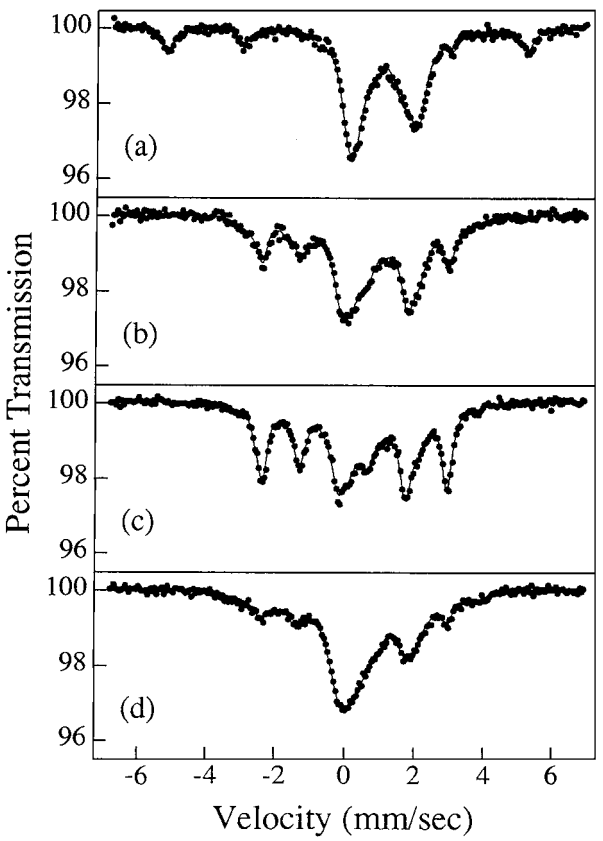

FIG. 10. Room-temperature Mössbauer spectra of prereduced 4% Fe/SiO_2 (calcined) after various reaction times: (a) $t = 0$ min, (b) $t = 50$ min, (c) $t = 160$ min, (d) $t = 750$ min.

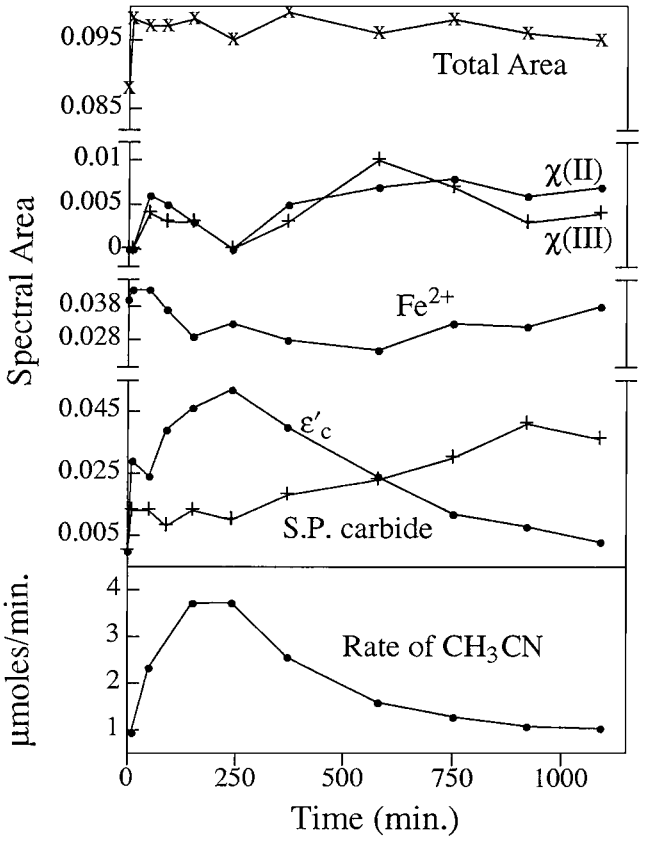

FIG. 11. Spectral areas and acetonitrile activity as a function of time on stream over prereduced 4% Fe/SiO_2 (calcined).

areas of ε' and χ carbides, obtained by fitting the spectra, are listed in Table 6. We note that the correction procedure adopted assumes a stoichiometric χ phase. The work of Le Caër and Bauer-Grosse (22) shows that increasing carbon content, indicated by the intensity of the $\chi^{(III)}$ component approaching that of the $\chi^{(II)}$ component, will lead to an underestimate of the amount of the ε' phase. The values in Table 6 show that this error has a relatively small effect on the shape of the ε' curve in Fig. 11.

After a 10-min exposure to reaction conditions, all the metallic iron and much of the low-coordination Fe^{2+} in the catalyst are carburized to form superparamagnetic carbide and some magnetically split ε' carbide. After 60 min of reaction, no surface Fe^{2+} is present and there is some formation of χ carbide. At longer reaction times, the ε' carbide is converted to χ carbide and then superparamagnetic carbide. Figure 12 shows the spectra collected at 298 and 103 K after 1090 min of reaction. The parameters of the fit are listed in Table 7. All the spectral areas except that of superparamagnetic carbide are higher at 103 K than at 298 K. However, the amount of magnetically split phase with hyperfine field characteristic of $\chi^{(II)}$ increases disproportionately, indicating a large contribution from θ carbide, which has a similar field. Thus, the superparamagnetic carbide appearing at longer reaction times corresponds to small domains of θ-Fe_3C. The acetonitrile activity shown at the bottom of Fig. 11 matches very well the trends of ε'_c carbide again, indicating that ε' carbide is the active phase of the catalyst. The initial maximum in the activity pattern can be interpreted as resulting from the slow conversion of surface Fe^{2+} to ε' carbide while the decay in activity results from the conversion of ε' carbide to lower-carbon-containing χ and θ carbides.

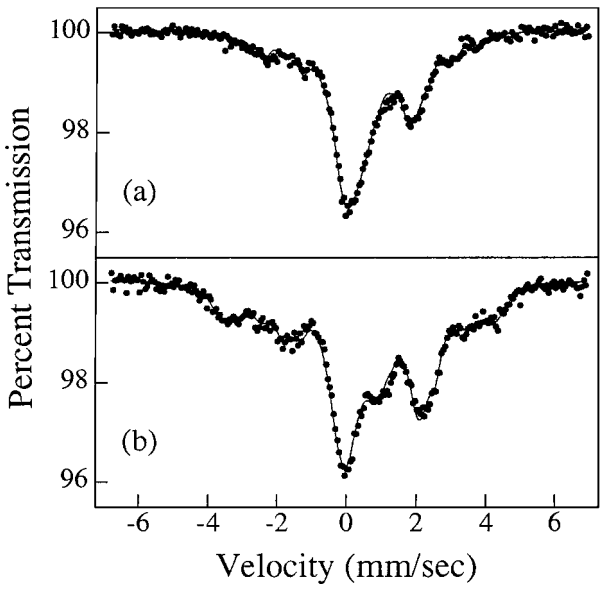

FIG. 12. Mössbauer spectra of prereduced 4% Fe/SiO_2 (calcined) after 1090 min of reaction at 698 K: (a) $T = 298$ K, (b) $T = 103$ K.

Active Phase of 4% Fe/SiO_2 (Reduced)

In situ Mössbauer studies on reduced 4% Fe/SiO_2 (reduced) give completely different results. Figure 13 shows

TABLE 7

Mössbauer Spectral Parameters Corresponding to Fig. 12 for Prereduced 4% Fe/SiO_2 (Calcined) after 1090 min of Reaction at 698 K

Fig.	Phase	IS (mm/s)	QS (mm/s)	HFS (kOe)	LW (mm/s)	Relative area (%)
12a	Fe^{2+}	0.93	1.8	—	0.80	36.5
	s.p. carbide	0.18	0.52	—	1.0	42.8
	ε'	0.24	0.02	161.9	0.33	7.0
	$\chi^{(I)}$	0.28	−0.1	182.8	0.30	4.8
	$\chi^{(II)}$	0.25	−0.08	219.2	0.35	5.1
	$\chi^{(III)}$	0.12	0.08	131.0	0.30	3.8
12b	Fe^{2+}	1.08	2.04	—	0.77	33.7
	s.p. carbide	0.32	1.07	—	0.87	23.2
	ε'	0.35	0.08	181.9	0.63	12.8
	$\chi^{(I)}$	0.40	−0.09	213.8	0.37	5.1
	$\chi^{(II)} + \theta$	0.33	0.0	244.9	0.76	20.7
	$\chi^{(III)}$	0.20	0.17	135.9	0.30	4.5

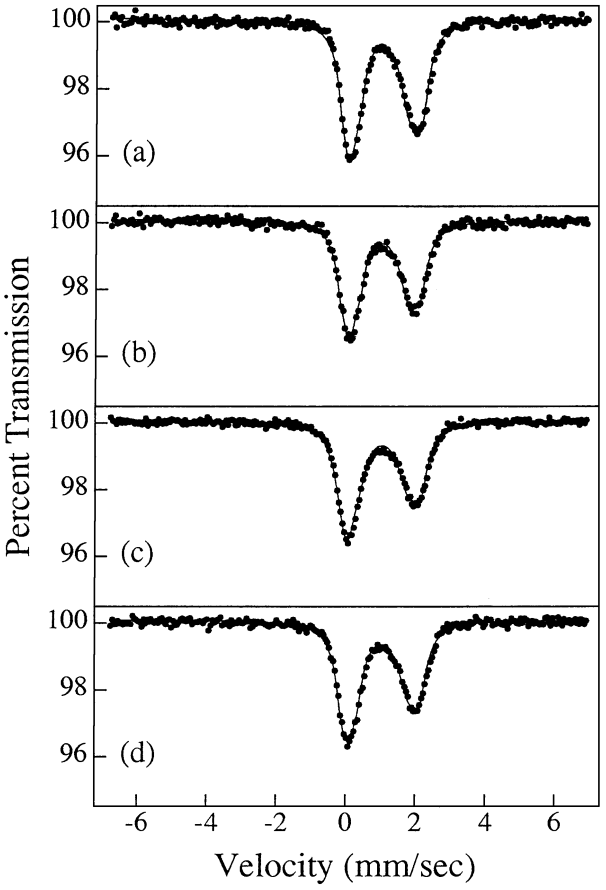

FIG. 13. Room-temperature Mössbauer spectra of prereduced 4% Fe/SiO_2 (reduced) after various reaction times: (a) $t = 0$ min, (b) $t = 160$ min, (c) $t = 865$ min, (d) $t = 1635$ min.

the room-temperature Mössbauer spectrum of reduced 4% Fe/SiO_2 (reduced) along with the spectra obtained after 160, 865, and 1635 min of reaction. Even after 26 h of reaction, the overall characteristics of the spectrum remain unchanged. There is no magnetically split phase visible in the room-temperature spectrum. Although the general appearance of the Mössbauer spectrum remains unchanged with time on stream, the activity starts very low and then gradually increases to a stable value. To get some qualitative information, the spectra were fitted with three doublets. The parameters of the fit are given in Table 8. Two of the doublets were assigned to the high-coordination or bulk Fe^{2+} (IS $\sim$ 1.1 mm/s, QS $\sim$ 2.1 mm/s) and low-coordination or surface Fe^{2+} (IS $\approx$ 1.0 mm/s, QS $\approx$ 1.6 mm/s). The third unknown doublet has parameters that are similar to those for superparamagnetic carbide (IS $\sim$ 0.12 mm/s, QS $\sim$ 0.55 mm/s). The changes in the spectral area of superparamagnetic carbide do not match very closely those for acetonitrile activity; however, there is a definite increase in the contribution of this species over the period of reaction. The slow rise in activity probably corresponds to a gradual conversion of some of the doublet corresponding to surface Fe^{2+} to another doublet corresponding to superparamagnetic carbide. A similar observation is made by Guczi and Lázár (26) for FeNaHX-zeolite samples, where in presence of $CO + H_2$ at 670 K, the iron species located in tetrahedral positions was converted to iron carbide. H_2 desorption measurements of postreaction 4% Fe/SiO_2 (reduced), using the method described by Amelse *et al.* (27), revealed 16% of iron in the metallic form after rereduction of used catalyst. This indicates that part of the Fe^{2+} phase was converted to carbide which, on rereduction, converted to Fe^0. Such conversion of surface Fe^{2+} to Fe^0 was also observed for 4% Fe/SiO_2 (reduced) when the catalyst was subjected to repeated cycles of reduction and nitriding (28). To examine the nature of the superparamagnetic carbide, the spectrum of the catalyst after 1635 min of reaction was also collected at 101 K; however, no magnetically split phase was seen at low temperature. The lack of any magnetically split phase indicates very low Debye temperatures for these surface species and also their small particle size. The high dispersion and intimate contact of nearly all the iron with the silica surface are implied by the appearance of all the iron in irreducible Fe^{2+} form in the Mössbauer spectrum.

Effect of Carburization on Activity

The acetonitrile activity for a variety of catalysts matches very well the amount of ε' carbide both in superparamagnetic form and in magnetically split form. Other authors have also observed correlations between activity and carbide formation during Fischer–Tropsch synthesis. Niemantsverdriet *et al.* (8) observed that at 513 K for the Fischer–Tropsch synthesis reaction, while the rate of product formation went through a maximum, the conversion of α-Fe into carbides started at a high rate and decreased

TABLE 8

Mössbauer Spectral Parameters Corresponding to Fig. 3 for Prereduced 4% Fe/SiO_2 (Reduced) after Various Reaction Times at 698 K

Fig.	Phase	IS (mm/s)	QS (mm/s)	HFS (kOe)	LW (mm/s)	Relative area (%)
13a	Fe^{2+} (low coord)	1.0	1.59	—	0.62	56.3
	Fe^{2+}	1.09	2.13	—	0.46	40.1
	Doublet-3	0.13	0.58	—	0.20	3.6
13b	Fe^{2+} (low coord)	0.97	1.64	—	0.65	59.7
	Fe^{2+}	1.09	2.07	—	0.48	33.1
	Doublet-3	0.13	0.60	—	0.26	7.2
13c	Fe^{2+} (low coord)	0.97	1.67	—	0.71	56.7
	Fe^{2+}	1.09	2.14	—	0.49	31.3
	Doublet-3	0.12	0.60	—	0.47	12.0
13d	Fe^{2+} (low coord)	0.98	1.65	—	0.7	57.7
	Fe^{2+}	1.08	2.11	—	0.48	32.7
	Doublet-3	0.11	0.50	—	0.32	9.6

rapidly. They attributed this behavior to a competition between bulk carbidization and hydrocarbon synthesis. Initially the rate of diffusion of carbon into α-Fe is very high. As more and more α-Fe is converted to carbides, however, the diffusion rate of carbon atoms into the catalyst slows down and progressively more carbon remains on the surface of the catalyst, forming hydrocarbon products and spots of graphite.

Raupp and Delgass (29) did simultaneous kinetic and single-velocity Mössbauer experiments and observed a linear relationship between the amount of bulk carbides formed and the rate of hydrocarbon formation during Fischer–Tropsch synthesis at 523 K. They explained this observation by a carbide model where the rate of product formation follows the carbide formation. Guczi and Lázár (26) have a completely different model in which the bulk carbide phase is the source of deactivation of the catalyst. They considered several iron environments that prevent bulk carbide formation, thereby maintaining the stable activity. One was stabilization of small iron particles by placing them in the geometrical constraints of a zeolite matrix. Other environments considered were formation of iron alloys and use of promoters that can prevent bulk carbide formation. In each of the above cases, the catalyst retained its activity. This indicated stabilization of small particles that provide active sites for dissociation of CO without forming bulk carbides.

In our case, both the competition model and carbide model can be used in explaining the trends of carbide and hydrocarbon and nitrile product formation. This is not surprising since the carbide model is a special case of competition model where the rate of carbide formation is much higher than the rate of product formation. In either model, however, bulk carbide formation acts as a getter for surface carbon, moderating the amount of active carbon at the surface. Mass spectral analysis of the step-change experiment on the reduced carbon-supported catalyst indicated that α-Fe converts to carbide before product formation starts. Perhaps the rate of carbide formation is very high compared with hydrocarbon and nitrile production and only as carbide formation nears completion is carbon available for product formation. This is consistent with the competition model. On the silica-supported catalysts, however, the activity increases for the first several hours as more ε' carbide is formed. In this case, the activity is directly dependent on the amount of ε' carbide present. This is consistent with the carbide model and the competition model at steady state. The assertion by Guczi and Lázár that bulk carbide formation is a source of deactivation is also true in the circumstances where the degradation of bulk carbide occurs during the course of reaction. In our experiments, the instability of ε' carbide at high reaction temperatures leads to loss of carbon from its lattice and thus a source of excess surface carbon that can block sites, with the resultant loss in activity.

CONCLUSIONS

The different activity patterns observed over different iron catalysts were studied using *in situ* Mössbauer spectroscopy. The initial high activity observed on carbon-supported catalysts is attributed to the presence of small superparamagnetic ε' carbide particles. We attribute the activity drop in the first hour as due to the loss in surface area accompanying conversion of superparamagnetic carbide to magnetically split ε' carbide. The drop in activity in later stages of reaction results from the conversion of ε' to χ and θ carbides. Spectra collected at cryogenic temperature after short reaction times confirm the order of carburization to be $Fe^0 \rightarrow \varepsilon' \rightarrow \chi \rightarrow \theta$. Transient step-change experiments on carbon-supported catalysts show formation of carbide before initiation of product formation. This fast rate of carbide formation makes it reasonable to discuss activity in terms of the phases present after reaction for times exceeding several minutes.

The rereduction of spent carbon-supported catalysts results in the production of relatively large particles of Fe^0. On further reaction, however, the rereduced catalyst quickly reverts to the form it had at the end of the preceding reaction period. Thus, irreversible processes such as sintering prevent major enhancement in the activity of the catalyst by intervening rereduction.

For the silica-supported catalyst containing both Fe^0 and Fe^{2+}, the initial rise in activity is caused by gradual conversion of surface Fe^{2+} to ε' carbide. The decay in activity again results from conversion of ε' to χ and θ carbides. On the catalyst containing only Fe^{2+}, the gradual rise in activity probably results from conversion of surface Fe^{2+} to small superparamagnetic carbide particles. Because of the low Debye temperature of these particles, however, a clear trend in phase behavior versus time was not observed by Mössbauer spectroscopy, but the presence of reduced iron after rereduction of an activated catalyst was confirmed by H_2 desorption experiments.

ACKNOWLEDGMENTS

We are grateful for support of this work by the National Science Foundation (Grant CBT 8519688) and a grant from Mobil Corporation. We also thank Haynes International for providing us the Haynes 230 alloy, Duane Klarstrom of Haynes International for valuable discussions about the alloy, and Weldon Vaughn at Chemistry Machine Shop, Purdue University, for fabrication of the Mössbauer cell.

REFERENCES

1. Olivé, G., and Olivé, S., U.S. Patent 4,179,462 (Dec. 19, 1979).
2. Gambell, J. W., and Auvil, S. R., U.S. Patent 4,272,451 (June 9, 1981).
3. Auvil, S. R., and Penquite, C. R., U.S. Patent 4,272,452 (June 9, 1981).
4. Hummel, A. A., Badani, M. V., Hummel, K. E., and Delgass, W. N., *J. Catal.* **139**, 392 (1993).
5. Butt, J. B., *Catal. Lett.* **7**, 61 (1990).

6. Raupp, G. B., and Delgass, W. N., *J. Catal.* **58**, 348 (1979).
7. Amelse, J. A., Butt, J. B., and Schwartz, L. H., *J. Phys. Chem.* **82**, 558 (1978).
8. Niemantsverdriet, J. W., van der Kraan, A. M., van Dijk, W. L., and van der Baan, H. S., *J. Phys. Chem.* **84**, 3363 (1980).
9. McDonald, M. A., Storm, D. A., and Boudart, M., *J. Catal.* **102**, 386 (1986).
10. Tau, L. M., Borcar, S., Bianchi, D., and Bennett, C. O., *J. Catal.* **87**, 36 (1984).
11. Loktev, S. M., Makarenkova, L. I., Slivinskii, E. V., and Éntin, S. D., *Kinet. Katal.* **13**, 1042 (1972).
12. Arents, R. A., Maksimov, Yu. V., Suzdalev, I. P., Imshennik, V. K., and Krupyanskiy, Yu. F., *Fiz. Metal. Metalloved.* **36**, 277 (1973).
13. Badani, M. V., Eshelman, L. M., and Delgass, W. N., *in* "New Frontiers in Catalysis: Proceedings, 10th International Congress on Catalysis, Budapest, 1992" (L. Guczi, T. Solymosi, and T. Tetenyi, Eds.), p. 1223. Akadémiai Kaidó, Budapest, 1992.
14. Chen, A. A., Vannice, M. A., and Phillips, J., *J. Phys. Chem.* **91**, 6257 (1987).
15. Delgass, W. N., Chen, L. Y., and Vogel, G., *Rev. Sci. Instrum.* **47**, 968 (1976).
16. Howsmon, G. J., Ph.D. thesis, Purdue University, 1992.
17. Hesse, J., and Rübartsch, *J. Phys. E* **7**, 526 (1974).
18. Wivel, C., and Mørup, S., *J. Phys. E* **14**, 605 (1981).
19. Mørup, S., Dumesic, J. A., and Tøpsoe, H., *in* "Applications of Mössbauer Spectroscopy" (R. L. Cohen, Ed.), Vol. II, p. 1. Academic Press, New York, 1980.
20. Niemantsverdriet, J. W., van der Kraan, A. M., Delgass, W. N., and Vannice, M. A., *J. Phys. Chem.* **89**, 67 (1985).
21. Gatte, R. R., and Phillips, J., *J. Catal.* **104**, 365 (1987).
22. Le Caër, G., and Bauer-Grosse, E., *Hyperfine Interact.* **47**, 55 (1989).
23. Le Caër, G., Dubois, J. M., Pijolat, M., Perrichon, V., and Busslère, P., *J. Phys. Chem.* **86**, 4799 (1982).
24. Jack, D. H., and Jack, K. H., *Mater. Sci. Eng.* **11**, 27 (1973).
25. Gager, H. M., and Hobson, M. C., Jr., *Catal. Rev. Sci. Eng.* **11**, 117 (1975).
26. Guczi, L., and Lázár, K., *Catal. Lett.* **7**, 53 (1990).
27. Amelse, J. A., Schwartz, L. H., and Butt, J. B., *J. Catal.* **72**, 95 (1981).
28. Badani, M. V., Ph.D. thesis, Purdue University, 1992.
29. Raupp, G. B., and Delgass, W. N., *J. Catal.* **58**, 361 (1979).